International Journal of Fatigue 80 (2015) 406–416

Contents lists available at ScienceDirect

International Journal of Fatigue

journal homepage: www.elsevier.com/locate/ijfatigue

Fatigue crack growth of a metastable austenitic stainless steel

D.F. Martelo [a,*], A.M. Mateo [b], M.D. Chapetti [a]

[a] INTEMA, Research Institute for Material Science, University of Mar del Plata-CONICET, J.B. Justo 4302 (B7608FDQ), Mar del Plata, Argentina
[b] CIEFMA – Dept. Ciencia de los Materiales e Ingeniería Metalúrgica, Universitat Politècnica de Catalunya, 08028 Barcelona, Spain

ARTICLE INFO

Article history:
Received 26 September 2014
Received in revised form 27 June 2015
Accepted 29 June 2015
Available online 3 July 2015

Keywords:
Fatigue crack propagation
Metastable austenitic stainless steel
Crack closure
ΔK and K_{max}
Martensitic transformation

ABSTRACT

The fatigue crack growth behavior of an austenitic metastable stainless steel AISI 301LN in the Paris region is investigated in this work. The fatigue crack growth rate curves are evaluated in terms of different parameters such as the range of stress intensity factor ΔK, the effective stress intensity factor ΔK_{eff}, and the two driving force parameter proposed by Kujawski K^*.

The finite element method is used to calculate the stress intensity factor of the specimens used in this investigation. The new stress intensity factor solution has been proved to be an alternative to explain contradictory results found in the literature.

Fatigue crack propagation tests have been carried out on thin sheets with two different microstructural conditions and different load ratios. The influence of microstructural and mechanical variables has been analyzed using different mechanisms proposed in the literature. The influence of the compressive residual stress induced by the martensitic transformation is determined by using a model based on the proposal of McMeeking et al. The analyses demonstrate the necessity of including K_{max} as a true driving force for the fatigue crack growth. A combined parameter is proposed to explain the effects of different variables on the fatigue crack growth rate curves. It is found that along with residual stresses, the microcracks and microvoids are other factor affecting the fatigue crack growth rate in the steel studied.

1. Introduction

The new environmental standard for the automotive industry requires the fabrication of more efficient vehicles with less fuel consumption. This technological challenge demands the development of new light weight materials. The metastable austenitic stainless steels (MASS) are materials with good formability and high strength compared to other carbon steels or aluminum alloys used in the automotive industry [1]. This high strength of MASS can be used to reduce the components thickness without decreasing vehicle safety.

The fatigue crack growth rate (FCGR) of MASS has been related to the martensitic transformation that occurs in the crack tip of this kind of steels [2–5]. The first study of fatigue crack propagation in steel with martensitic transformation in the crack tip was published by Chanani et al. [6]. The results of this work shows a decrease in the fatigue crack growth rate for the same range of stress intensity factor ΔK, when the austenitic structure was more unstable. Same result was obtained later by Pineau and Pelloux [2] in an austenitic metastable stainless steel AISI 301. The authors of both studies try to relate the decrease in the crack growth rate with the higher strain hardening coefficient of the more unstable alloy. To prove their hypothesis, the authors used a fatigue crack propagation model proposed by Head [7], and a fatigue crack propagation model proposed by Chanani et al. [6]. However, the crack propagation models used in both studies to establish a relationship between crack growth rate and ΔK exhibited an opposite tendency. Chanani's model predicts an increase in the FCGR with the increase in the work hardening, whereas Head's model predicts the opposite. Even in the case when the crack propagation in Head's model predicts a decrease in crack growth rate with the increase in work hardening coefficient, experimental results show differences with the prediction of the model.

Another mechanism used to explain the decrease in the FCGR associated to the martensitic transformation is the role of microstructure in the FCGR. To prove this hypothesis, Pineau and Pelloux [2] and Mei and Morris [3], in different studies, have compared the FCGR in the same alloy but under different conditions:

(a) Martensitic transformation induced by stress or strain during fatigue test *vs.* Martensite formed by quenching (1).

* Corresponding author.
E-mail address: martelo@fi.mdp.edu.ar (D.F. Martelo).

http://dx.doi.org/10.1016/j.ijfatigue.2015.06.029
0142-1123/

(b) Martensitic transformation induced by stress or strain during fatigue test *vs.* Martensite formed by cold rolled (2).

In both cases the FCGR for the same ΔK was higher for the specimens in which the structure was transformed to martensite previous to the fatigue test. These results suggest that the decrease in the FCGR is associated to the martensitic transformation during crack propagation rather than to the existence of a martensitic structure in the crack path.

Though the studies on the subject show the importance of martensitic transformation in the FCGR, the role of the martensitic transformation in mechanical variables that influence the FCGR, like load ratio *R*, is not clear. It has been suggested that martensitic transformation can induce crack closure, and this phenomenon could be used to explain the effects of load ratio and martensitic transformation on FCGR of AMSS. However, there is a lack of appropriate and systematic research on the contribution of crack closure to the crack growth rate in MASS.

The analysis of previous studies on the fatigue crack growth (FCG) in thin sheet specimens of MASS show the influence of mean stress in the FCGR for the same *R* and the same ΔK, in tests realized to constant *R* [4,8]. This is opposite to the behavior observed in thick specimens of MASS or to the common behavior reported for many alloys. This uncommon behavior will be discussed in this paper.

The present work will focus on the fatigue crack grow rate behavior of MASS in thin sheet specimens. The influence of martensitic transformation and mechanical variables on FCGR will be analyzed in the Paris region of FCG. In addition to the mechanism introduced above, another mechanism to explain the influence of the martensitic transformation in the FCGR is discussed.

2. Specimen, material, and testing

The material employed in the current study was an austenitic stainless steel AISI 301LN provided by OCAS NV, Arcelor-Mittal R&D Industry Gent (Belgium). The material was provided in thin sheet specimens of 1 mm and 1.5 mm thickness, in two different conditions: annealed and cold rolled (40% degree of cold rolling). The chemical composition of the material used is shown in Table 1. The mechanical properties with the transformation temperatures are shown in Table 2.

To reveal the microstructure, the material was grounded in the surface with SiC emery paper up to a roughness of 1200 grit and then polished. Since the mechanical grinding can induce martensitic transformation, the material was electro-polished with a solution consisting of 5 vol% perchloric acid and 95% ethanol at 45 V for 15 s. The austenite phase was revealed by electro-etching in a solution of 65% acid nitric at 1.2 V. Fig. 1a shows an homogeneous structure composed by equiaxial austenitic grains with an average grain size of 11.8 μm. Fig. 1b shows the austenitic grain oriented in the rolling direction. X-ray diffraction measurements showed that the cold rolled steel has a percentage of martensite that is approximately 38 ± 5%.

The same procedure used to reveal the microstructure was repeated for all specimens tested in order to observe the martensitic transformation around the crack tip. The martensite phase was revealed by chemical etching in a solution of 100 ml ethanol, 20 ml HCl, 1.5 g $K_2S_2O_5$ and 2 g $NH_4F{\cdot}HF$.

The FCG tests were carried out on single edge notch tension specimens (SENT). The width of the specimens was 35 mm and 40 mm, and the total length of most specimens was 25 cm.

Table 1
Chemical composition (wt.%).

	Fe	Cr	Ni	Mo	C	Si	P	S	Mn	Cu	N
Annealed – 1 mm	Bal	17.86	6.42	0.24	0.015	0.471	0.031	0.007	1.495	0.173	0.094–0.145
Annealed – 1.5 mm	Bal	17.98	6.78	0.23	0.012	0.548	0.031	0.004	1.562	0.057	0.094–0.145
Cold-rolled – 1.5 mm	Bal	17.94	6.30	0.18	0.016	0.513	0.032	0.005	1.481	0.135	0.094–0.145

Table 2
Mechanical properties with transformation temperatures.

	σ_{ys} (MPa)	σ_{UTS} (MPa)	Total elongation (Pct)	Ms (°C)	M_{d30} (°C)	M_d (°C)
Annealed – 1 mm	343	973	42.9[a]	−78.21[b]	40.89[b]	100[c]
Cold rolled – 1.5 mm	1120	1207	20.5[a]	−76.62[b]	42.57[b]	100[c]

[a] Tensile tests were carried out in subsize specimen (dimensions according to standard E 08-01).
[b] The Ms and the M_d temperatures are calculated using equations taken from Ref. [9], to make the calculation, the average value of *N* was used.
[c] M_d temperature for AISI 301 stainless steel [2].

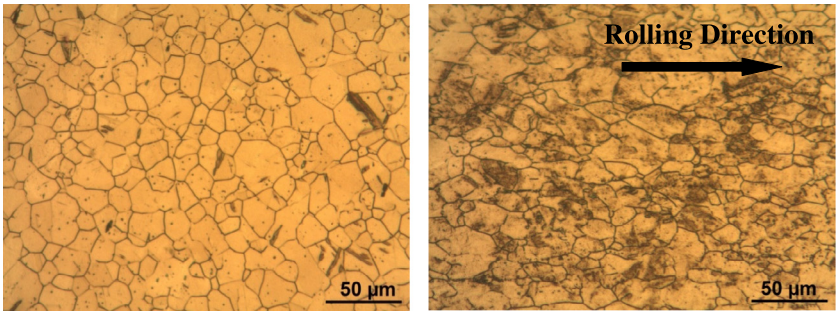

Fig. 1. Microstructure of an austenitic metastable stainless steel AISI 301LN: (a) annealed; (b) cold rolled. (In both pictures the thickness of the sheets is perpendicular to the micrographs.)

The specimens were held in wedge grips and the tests were conducted using an Instron Machine model 8801 with closed loop to computers for automatic test control and data acquisition. The crack extension was measured with krak-gages®, which is principally an indirect DC potential measurement technique. The krag-gages® theory is explained in Ref. [10]. The crack length was also measured using the compliance technique by means of a clip gage in the crack mouth and a strain gauge fixed in the back surface.

To measure the crack opening load, a procedure based on the compliance offset method proposed in the ASTM standard E647-08$^{\varepsilon 1}$ [11] was used. Unlike the compliance offset method where, the open-crack compliance corresponds to the compliance taken from fully-open crack configuration in the unloading curve. In the proposed procedure, the open-crack compliance corresponds to the average of the compliance taken from fully-open crack configuration of the curve in loading and unloading. Moreover, the compliance of the segments of the curve that spans a range 10% of the cycle load is taken from the average of the curve on loading and unloading part. The compliance offset is measured as in expression (1). The details of the compliance offset method are shown in detail in the ASTM standard E47-08$^{\varepsilon 1}$ [11]. From now on, the new method will be referred as "modified ASTM method". The signal noise was reduced by averaging 100 consecutive cycles and using low-pass digital filter [12,13]. The sampling rate used was of 400 data pairs (load and displacement) per cycle according the recommendations made by Song et al. [14].

$$\text{Compliance offset}\ (\%) = \frac{[(\text{open} - \text{crack compliance}) - (\text{compliance})]}{(\text{open} - \text{crack compliance})} \quad (1)$$

3. ΔK expressions

Paris et al. [15] formulates the first successful relationship between fatigue crack advance and cycles number through fracture mechanic's parameters. The success of this relationship was that it allowed establishing a one to one relationship between FCGR and ΔK for a defined load ratio regardless the stress applied. However there exist some studies in which the Paris' law was not satisfied [4,8]. In those studies, the FCG tests were conducted in thin specimen of MASS on SENT specimens, the same condition studied in this work. A possible explanation to that discrepancy is proposed in this investigation.

When wedge grips are used to support SENT specimens, a bending moment is induced in the specimen ends. This constrain causes a non-uniform stress distribution across the specimen, as shown in Fig. 2. The problem of wedge grips restricting free rotation was recognized by Adair et al. [16] who used a boundary element solution for a specimen with a uniform displacement boundary condition which is the case for wedge loading. They also validated their solution by showing that the results were indistinguishable from those obtained using a traditional SENT specimen. Therefore, the stress intensity factor tabulated in traditional books is not appropriate for SENT specimens supported with wedge grips; this equation proposed in handbooks is represented in Fig. 3 by the curve colored in red. For this reason, the finite element method (FEM) was employed to obtain the value of the stress intensity factor. John et al. [17] reported other method to calculate the stress intensity factor in single edge cracked geometries. The type of element used was CPS8R in a spider web arrangement.

Fig. 3 shows the stress intensity factor solution for two of the SENT specimen configurations that have been used for tests. The curve was normalized by dividing the stress intensity factor by the applied stress and the crack length by the specimen width.

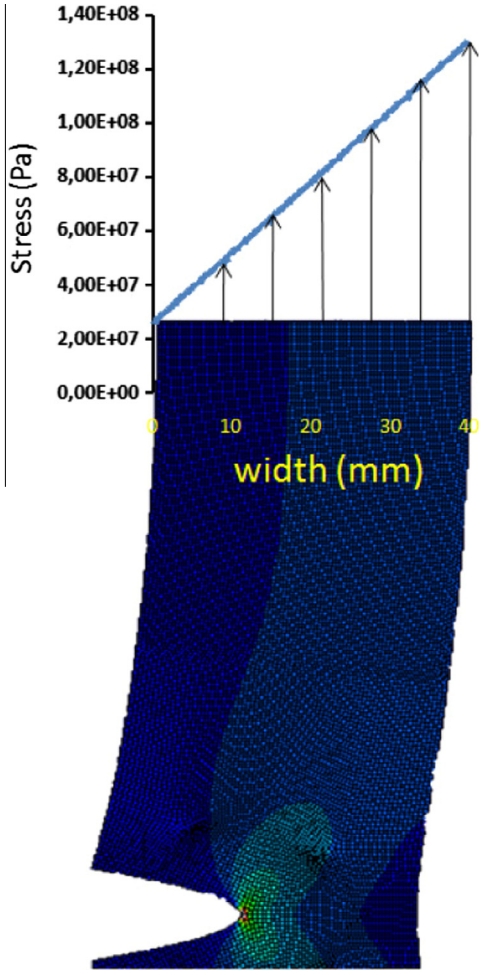

Fig. 2. Characteristic profile of the stresses applied along the edge of the SENT specimens of this study.

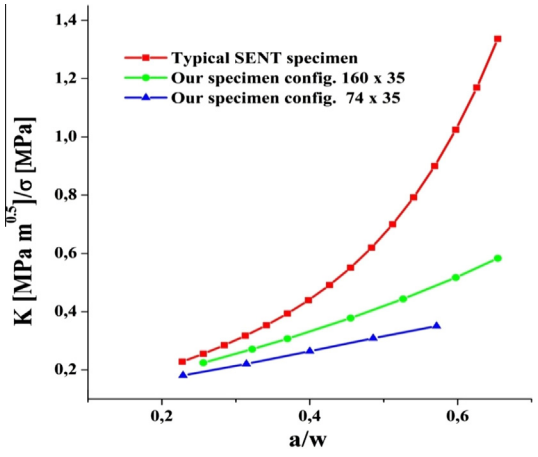

Fig. 3. Stress intensity factor solution *vs.* crack length. For SENT specimen of two different lengths and for typical SENT specimen.

The results obtained show that for the SENT specimens with wedge grips, the stress intensity factor depends on the size of the specimen.

Fig. 4 shows the relationship between fatigue crack growth rate *vs.* ΔK when the stress intensity factor (SIF) solution used is the one found in the handbooks, and when the stress intensity factor used

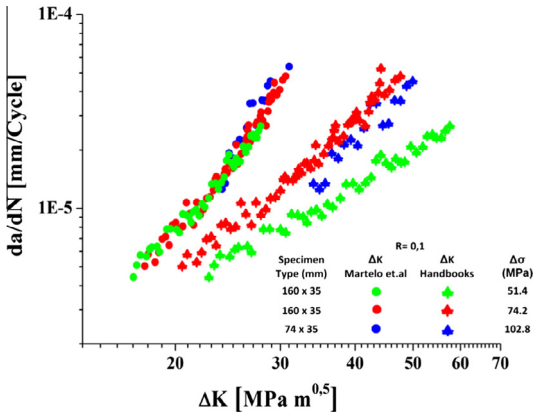

Fig. 4. Fatigue crack growth rate *vs.* stress intensity factor range for a load ratio of 0.1 using the SIF solution proposed in this study and the SIF solution proposed in handbooks [18].

is the one obtained by FEM. When using the stress intensity factor of the handbooks for specimens of the same size, there is an apparent increase of the FCGR with an increase in the applied stress for the same ΔK and the same load ratio. This dependency disappears when a proper stress intensity factor solution is used. This rationalization may be used to explain the contradictory results found in the literature [4,8] which show that in thin sheet SENT specimens of MASS, the FCGR increases with the increase of the applied stress.

4. Results

4.1. Fatigue crack growth rate curves in terms of the range of stress intensity factor

Fig. 5 shows the fatigue crack growth rate *vs.* ΔK of an austenitic stainless steel AISI 301LN in annealed condition (Fig. 5a) and cold rolled condition (Fig. 5b). In all cases, an increase in the FCGR with an increase of ΔK and with an increase in K_{max} for the same ΔK can be observed. For a given ΔK and load ratio, the FCGR is independent of the mean stress. The FCGR curve for a constant R is always lower for the annealed steel compared to the cold rolled steel. For the cold rolled, the influence of crack plane orientation is negligible.

4.2. FCGR curves in terms of K_{eff} and two driving force parameters

To explain the differences in FCGR curves as a consequence of load ratio, the crack closure has been chosen as the principal mechanism responsible [19]. This mechanism has also been used in the past to explain the difference in FCGR among different microstructural conditions [20]. According to the traditional concepts of crack closure proposed by Elber [21], the effective driving force for FCGR is defined as:

$$K_{eff} = K_{max} - K_{op} \tag{2}$$

Fig. 6 shows the plots of FCGR *vs.* ΔK_{eff} for the annealed steel using different methods to define the crack opening load (P_{op} or K_{op}) and different offsets. When K_{op} is defined using a 2% offset (Fig. 6a), K_{eff} loses meaning as driving force. This is concluded because in the FCGR curve at $R = 0.1$ and $\Delta P = 2.6$ kN, an injective function between ΔK_{eff} and FCGR cannot be established. The FCGR can be better expressed in terms of ΔK_{eff} using an offset of 4% as shown in Fig. 6b.

As it occurs in the Paris region for the annealed steel, the crack closure cannot explain the effects of the load ratio on the FCGR of the cold rolled steel (Fig. 7). In this case, it is even more difficult to explain the difference in the FCGR based on crack closure concepts, since at R equal to 0.3 and R equal to 0.5 the crack closure phenomenon is not present.

Another rationalization used to explain the load ratio effects are the concepts based on two driving forces as proposed by Kujawski [19]. The Kujawski's parameter is based on the fact that both K_{max} and ΔK contribute to the crack growth, and for several alloys, this author has shown that the relationship of Fig. 8 is satisfied [19].

The Kujawski's parameter is calculated as follows:

$$K^* = (K_{max})^{\alpha}(\Delta K^+)^{1-\alpha} \tag{3}$$

where ΔK^+ is the positive part of the range of the stress intensity factor and α is a factor that determines the importance of K_{max} and ΔK, α is calculated by means of the following expression:

$$\alpha = \frac{\log(\Delta K_1/\Delta K_2)}{\log((1-R_1)/(1-R_2))} \tag{4}$$

The average value of α for the AISI 301LN in annealed condition is 0.6, while for the AISI 301LN in cold rolled condition is 0.7. These results shows that Kujawski's parameter can successfully correlate the load ratio effects for the steels in annealed and cold rolled condition, as seen in Fig. 9a and b. Unfortunately, the driving forces for fatigue crack growth (ΔK, K_{max}, K^*, ΔK_{eff}), which are usually calculated using only the load, the crack length and the geometry of the specimen, can be substantially modified from the nominal values by factors like crack deflection [22], or residual stresses [23],

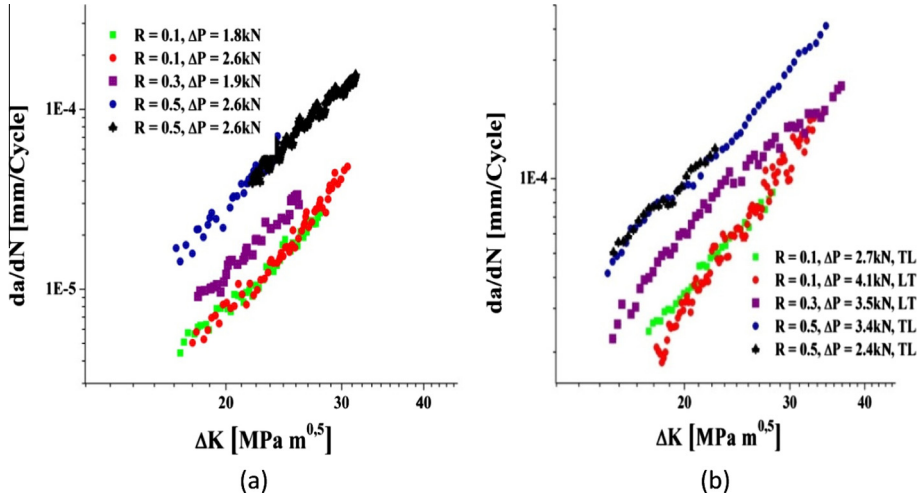

Fig. 5. Fatigue crack growth rate *vs.* stress intensity factor range at different load ratio (a) in the annealed steel (b) in the cold rolled steel.

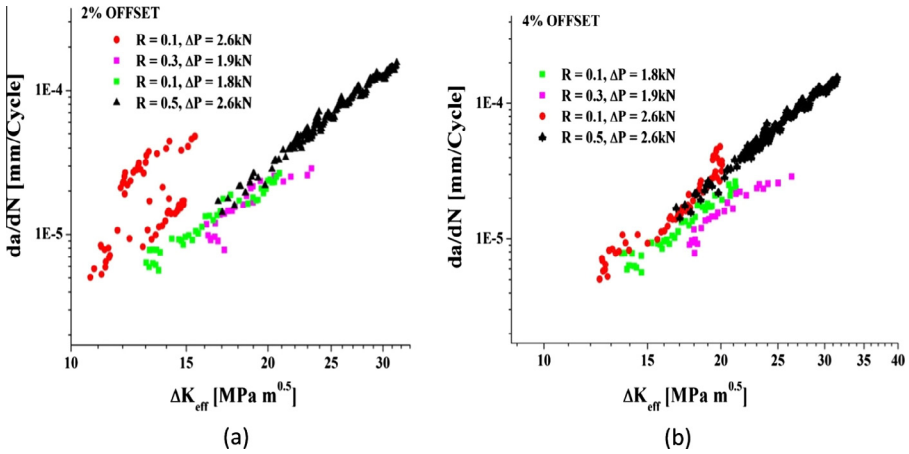

Fig. 6. Fatigue crack growth rate as a function of the effective stress intensity factor defined using the method: (a) modified ASTM with offset of 2%, (b) modified ASTM with offset of 4%.

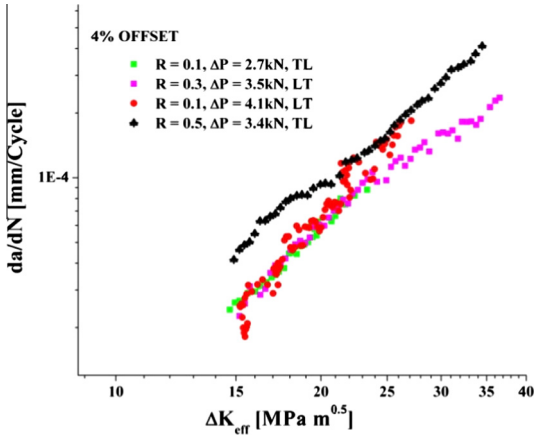

Fig. 7. Fatigue crack growth rate as a function of the effective stress intensity factor for the cold rolled steel.

among others variables. The correct estimation of the true driving force is a necessary step to explain the microstructural effects on the FCGR.

5. Martensitic transformation zone

Different methods have been implemented in order to quantify the austenite transformed to martensite as a result from an applied stress or strain. These includes: X-ray diffraction, magnetic measurements and optical measurements, among others [3,24–27]. In tensile tests, the magnetic measurement using a Ferritescope has proved to be very successful. Even though the Ferritescope must be calibrated, the calibration factor has been reported to be ≈1.7 in two independent studies carried out in an AISI 301LN [24,25]. The in situ Ferritescope measurements must be performed in stress free conditions [24], that it is only possible in fatigue test with load ratio $R = 0$. The X-ray diffraction measurements are texture dependent, and compared to Ferritescope measurements the results are poor [24,25]. With respect to the optical measurements, this technique shows to be inexact and time consuming [25]. Authors think that the optical technique is the more adequate to obtain local measurements from the martensitic transformation around a fatigue crack.

Measurements of the martensite around a crack after fracture toughness and fatigue tests have been performed using optical metallography in Refs. [3,26,27]. In these studies the martensite has been revealed by chemical etching or by using Ferrofluid. Only one of these studies showed quantitative measurements of the martensitic transformation zone [3], in which the martensitic transformation zone is proportional to ΔK and R. Besides, the size of the transformation zone in front of the crack tip is proportional to the equivalent shear stress.

In this study different techniques were used to determine and measure the martensitic transformation around the crack. X-ray analysis were conducted on the fatigue fracture surface of the MASS in some of the different conditions tested, see Fig. 10. The diffractograms do not show evidence of the austenite phase on

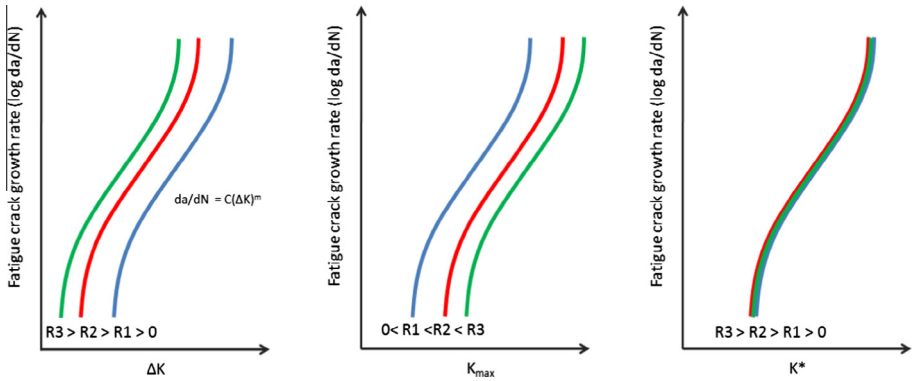

Fig. 8. Schematic representation of the FCGR as a function of ΔK, K_{max} and K^*.

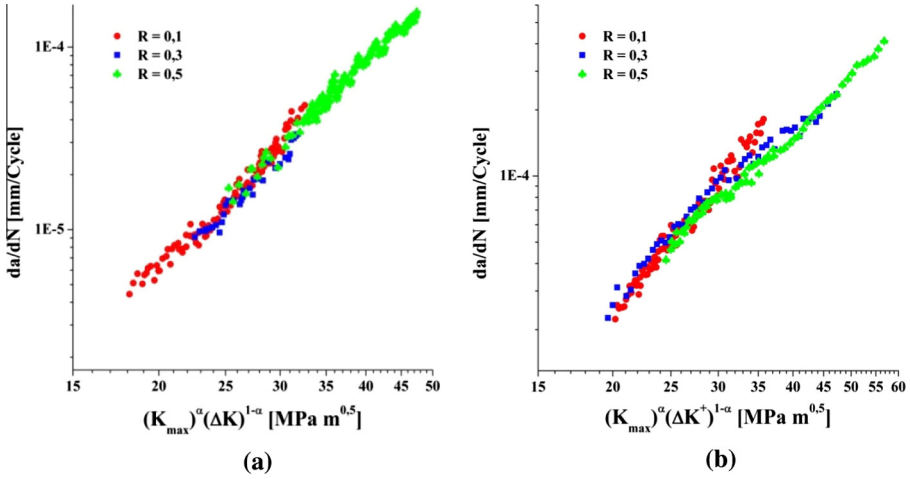

Fig. 9. Fatigue crack growth rate as a function of the Kujawski's parameter for (a) the annealed steel (b) the cold rolled steel.

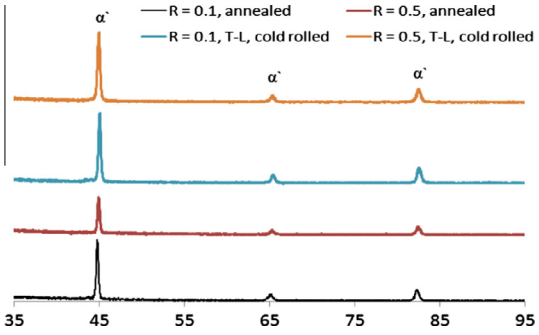

Fig. 10. X-ray diffraction spectra of the fracture surface in the annealed steel and in the cold rolled steel.

the surface fracture, which indicates that very close to the crack, the martensitic transformation is complete.

Optical micrographs (etched) of the fatigue crack tip can be seen in Fig. 11a–d. In this micrograph the martensite is colored darker than the austenite. From the complete analysis of the micrographs, some features are worth mentioning:

i. There is no martensitic transformation in front of the crack tip beyond the last grain that is traversed by the fatigue crack.
ii. There is no martensitic transformation, even in zones of partial martensitic transformation, caused by the crack advance beyond the 200 μm from the crack.
iii. The martensitic transformation zone is bigger in the annealed specimen than in the cold rolled specimen.
iv. The zone of complete martensitic transformation is proportional to the range of stress intensity factor (ΔK), rather than the maximum stress intensity factor (K_{max}).

With respect to comment (iii), it is worth noting that the cold rolled steel is not necessarily much more stable than the annealed steel. For example, Table 3 shows the volume of martensite transformed during tensile tests at room temperature for AISI 301LN

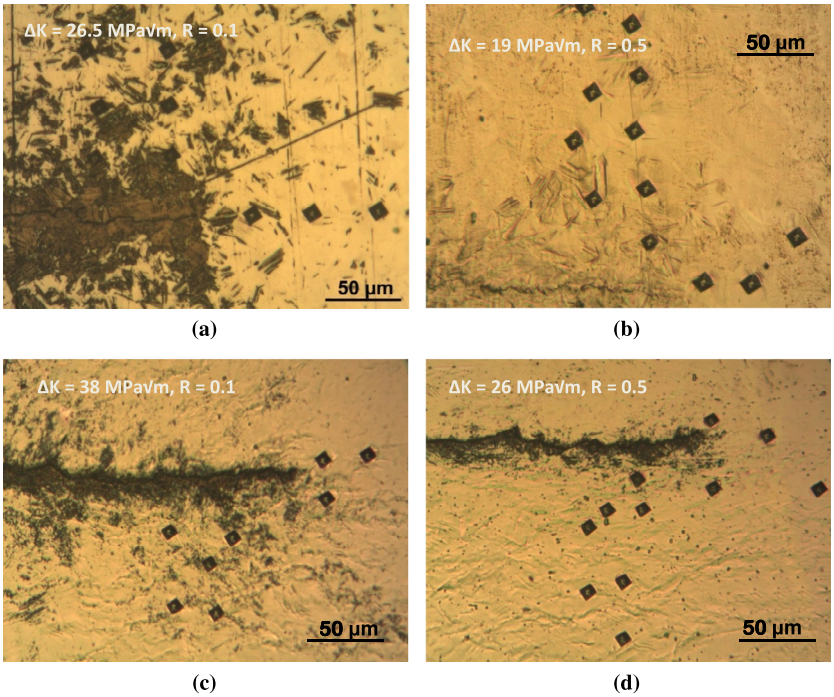

Fig. 11. Optical micrographs of the fatigue crack profile showing the martensite phase in black (a and b) annealed steel, (c and d) cold rolled steel.

Table 3
Volume fraction of austenite transformed to martensite in an MASS AISI 301LN in two different conditions. The martensite content was reported at elongation to failure.

Condition	Volume fraction of martensite (%)		
	Prior to test	New martensite	Total content
Annealed	0	87.9	87.9
20% Cold rolled	20	70	90

steel in two conditions: annealed and 20% cold rolled from the papers [1,28], respectively. This table shows that for both materials the maximum percentage of austenite transformed to martensite can be very high, around 90%.

Furthermore, the authors consider that the higher level of martensite in the annealed steel is not only related to the stability of the material. For the cold rolled steel for the period of fatigue crack propagation, the material damage can be confined to a smaller zone (higher yield stress, so smaller plastic zone) and therefore the zone of martensitic transformation is smaller.

All characteristic previously mentioned were confirmed by the micro-indentation technique, as it can be seen in Fig. 11a–d. In this micrograph it is highly evident that the indentations next to the crack are smaller than the indentation in front of the crack tip. The height of the zone of complete martensitic transformation can be described by the material in annealed condition (ZT_a) and cold rolled (ZT_c) condition by the following Eqs. (5) and (6), respectively.

$$ZT_a\ [\mu m] = 2.672\Delta K - 28.36 \tag{5}$$

$$ZT_{cr}\ [\mu m] = 0.22\Delta K + 3.87 \tag{6}$$

6. Discussion

6.1. Crack path profile analysis

Based on the experimental results of this paper, it is not possible to explain the differences in the FCGR between annealed and cold rolled specimens based on crack closure. It is neither possible to explain the difference in FCGR based on the existence of an extensive harder structure in front of the crack, like the martensite, or based on the increase in the work hardening, as explained above. However, there are other mechanisms that have been studied by others, which can contribute to explain the effects of martensitic transformation on the FCGR of MASS. Based on the success of Kujawski's parameter to explain the load ratio effects, any other mechanism used to explain the FCG behavior of this kind of steels should not ignore the contribution of K_{max} as part of the total driving force.

It is well known that the microstructural characteristics are very important in the FCGR when the cyclic plastic zone is of the same dimension than the size of the microstructural characteristic size (near fatigue threshold). However, the interaction of a new coherent or semi coherent interface, like the austenite–martensite, could promote crack deflection. Roughness can decrease FCGR through three mechanisms: (i) for the same over-all crack length, the effective crack length is larger for rougher cracks which implies more energy for the creation of a new surface fracture; (ii) for the same crack, a rougher crack reduces the effective driving force; (iii) roughness can induce crack closure [22]. Fig. 12a–d shows the crack profile of different specimens tested under different conditions. The existence of crack branching in the whole range of ΔK applied can be observed, being more pronounced in the region of higher values of ΔK. For all cases, the crack path is irregular. The peaks of roughness R_g are a little bigger than the microstructural characteristic size, although the typical roughness is of the same order of magnitude than the microstructural characteristic size.

Due to the fact that the crack profiles of the different conditions tested did not show any particular characteristic, and because no appreciable difference was found in crack roughness, it is not possible to use this mechanism to explain the difference in FCGR among the different microstructural conditions studied.

6.2. Stress field induced by the martensitic transformation

According to McMeeking and Evans [29], an increase in the toughness of some brittle materials like Zirconia could be generated by the reduction in the crack opening displacement caused by an expansive transformation. In his original paper, McMeeking and Evans [29] calculated the stress intensity factor caused by the martensitic transformation. Mei and Morris [3], used the same idea to explain the decrease in the FCGR of an austenitic stainless steel AISI 304 at transformation temperature. However, in both cases they calculated the stress intensity factor caused by the martensitic transformation considering the existence of a zone of martensitic transformation in front of the crack tip.

In MASS like the AISI 304, the martensitic transformation causes a volume expansion of 2% [30]. To determine the stress intensity factor induced by the compressive stresses of the martensitic transformation, the weight function method proposed by Paris et al. [31] is used.

$$K_{tran} = \int_S T \cdot h dS \tag{7}$$

where T are the tensions applied along the contour S, if only the volume expansion is considered, then the tension T will be

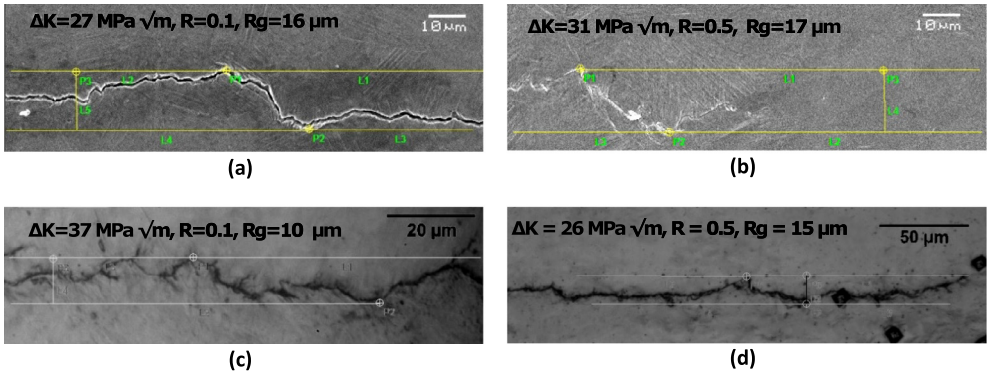

Fig. 12. Optical and scanning electron micrographs of crack profile in a metastable austenitic stainless steel in (a and b) annealed condition and (c and d) cold rolled condition.

perpendicular to S. h is a weight function and K_{tran} is the stress intensity factor caused by the martensitic transformation. The results obtained using the weight function are limited to the region very close to the crack. The function h is given in Ref. [31] and it is defined as follows:

$$h_x = \frac{\cos\frac{\theta}{2}(4\upsilon^* - 2 + \cos\theta - \cos 2\theta)}{4\sqrt{2\pi}(1-\upsilon)\sqrt{r}}$$
$$h_y = \frac{\sin\frac{\theta}{2}(4 - 4\upsilon^* - \cos\theta - \cos 2\theta)}{4\sqrt{2\pi}(1-\upsilon)\sqrt{r}} \quad (8)$$

for plane stress $\upsilon^* = \upsilon(1+\upsilon)$ and T can be expressed as [29]:

$$T = pn = p(n_x + n_y) \quad (9)$$

where p is the stress generated by the volume expansion. Taking into account that the experimental observations from this study do not show a zone of martensitic transformation in front of the crack tip, the calculation of stress intensity factor will be done following a contour S as shown in Fig. 13.

Therefore, the equation to be solved for each segment is as follows:

$$K_{tran} = p\int_S n\cdot h dS = p\int_S (n_x h_x + n_y h_y) dS \quad (10)$$

The stress intensity factor obtained from the contribution of all segments is plotted against the crack length normalized by the height of the zone of martensitic transformation, Fig. 14.

When the crack length is much bigger than the height of the zone transformed to martensite, the curve in Fig. 14 approaches an asymptotic value. Eq. (11) represents the decrease in the stress intensity factor due to zone of austenite completely transformed to martensite as observed in this material for the tests conducted.

$$K_{tran} = K_1 + K_2 + K_3 + K_4 \Rightarrow K_L \overset{a\to\infty}{\to} -0.608\frac{p}{(1-\upsilon)}\sqrt{ZT} \quad (11)$$

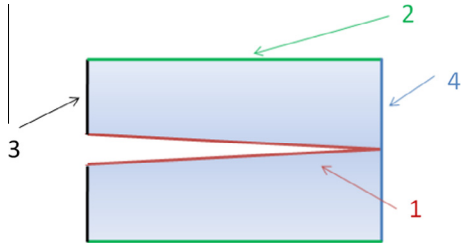

Fig. 13. Schematic contour of the martensitic transformation around a fatigue crack in a MASS AISI 301LN.

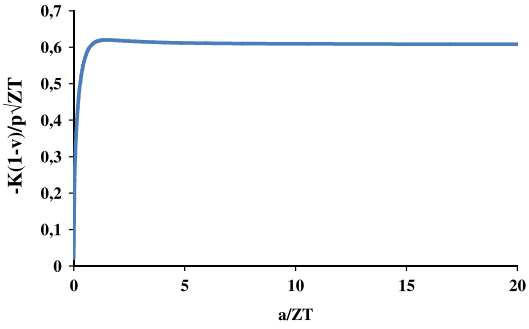

Fig. 14. Resistance curve caused by the martensitic transformation adjacent to the crack.

Eq. (11) implies that the transformation from austenite to martensite affects the FCGR, even when the distribution of martensite is not present ahead of the crack tip.

Besides, the most popular predictive model proposed to estimate the lifetime in components containing cracks and subjected to variable loads are based on ΔK as a driving force, and for example, in the Paris equation, the effect of the load ratio is taken into account through different values of a material constant C. However, in order to reduce the number of constants, the choice of a proper driving force is necessary. The expressions (12) and (13) will show that ΔK is not affected by K_{tran}, and therefore, this parameter is not suitable to estimate the effects of the martensitic transformation. We know that:

$$\Delta K = K_{max} - K_{min}$$
$$\text{or} \quad (12)$$
$$\Delta K_{eff} = K_{max} - K_{cl}$$

Considering that ΔK_{eff} is not appropriate to characterize the FCGR in this kind of material, as previously shown, and after adding the contribution of the martensitic transformation as a driving force, we obtain:

$$K_{min\ tran} = K_{min} - K_{tran}$$
$$K_{max\ tran} = K_{max} - K_{tran}$$
$$\Delta K_{tran} = K_{max\ tran} - K_{min\ tran} = (K_{max} - K_{tran}) - (K_{min} - K_{tran)} = \Delta K \quad (13)$$

Because K_{tran} does not contribute to ΔK parameter, and based on the fact that a two-driving-force parameter is very successful in explaining the load ratio effects, the following combined parameter is proposed to do so, as well as to explain the effect of martensitic transformation in the FCGR of MASS:

$$K_m^* = (K_{max} - f(x))^{\alpha_n}(\Delta K^+)^{1-\alpha_n} \quad (14)$$

In this particular case:

$$K_m^* = (K_{max\ tran})^{\alpha_n}(\Delta K_{tran}^+)^{1-\alpha_n}$$
$$\text{or} \quad (15)$$
$$K_m^* = (K_{max} - K_{tran})^{\alpha_n}(\Delta K^+)^{1-\alpha_n}$$

where α_n is a parameter with the same physical meaning of the parameter α. The value of p used to calculate K_{tran} was taken from the experimental value obtained by Rajanna et al. [32], who measured the residual stresses in the martensite and austenite phases of the surface fracture of an MASS AISI 304 and AISI 316. The determination of α_n is performed by using the equation (4), however, in this case the values of $R_1 = K_{min1}/K_{max1}$ and $R_2 = K_{min2}/K_{max2}$ that must be used are $R_1 = K_{min\ tran1}/K_{max\ tran1}$ and $R_2 = K_{min\ tran2}/K_{max\ tran2}$. The values of α_n results to be 0.5 and 0.6 for the steel in annealed condition and cold rolled condition, respectively. Fig. 15 compares the results obtained using Kujawski's parameter versus the parameter proposed in Eq. (15). It can be observed that the K_m^* tends to join the curves together. The difference in the FCGR between the MASS in annealed condition and the one in cold rolled condition can be partially explained if the value of p is equal to $C = LB\varepsilon^t$ ($L = 0.5$, B is the bulk elastic modulus of the martensite, and ε^t is the volumetric strain of the martensitic transformation), as explained by Biswas et al. [5]. The results obtained using that value of p and values of α_n equal to 0.5 and 0.6 for the steel in annealed condition and cold rolled condition respectively are shown in Fig. 16a for a load ratio of 0.1. The values of K_{tran} for both analysis are shown in Fig. 17. The inferior limit is for the calculation according to results of Rajanna et al. [32] and the upper limit for the calculation according to estimation of Biswas et al. [5].

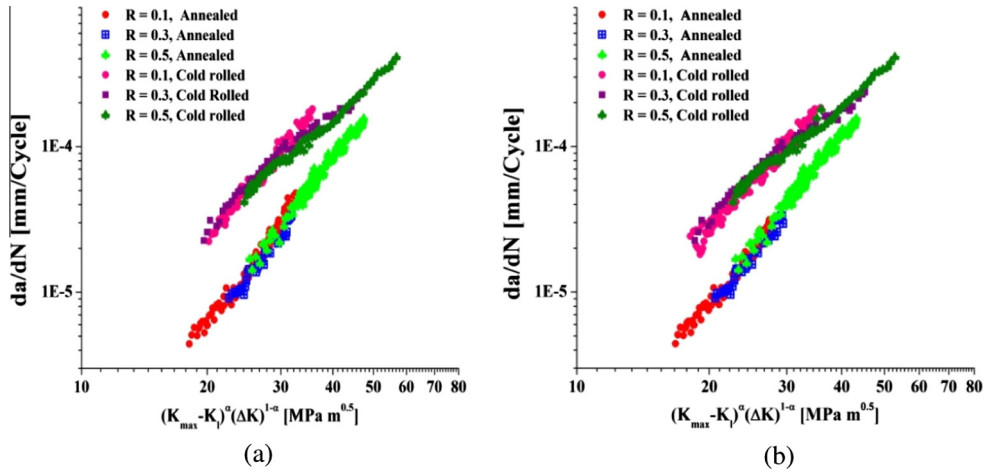

Fig. 15. Fatigue crack growth rate as a function of (a) the Kujawski's parameter (b) the Kujawski's parameter modified by the compressive stresses generated by the martensitic transformation.

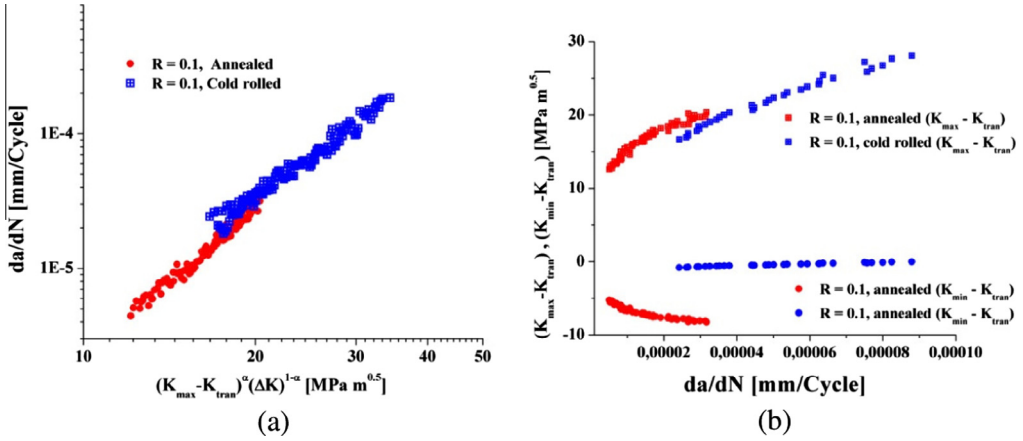

Fig. 16. (a) Fatigue crack growth rate as a function of the Kujawski's parameter modified by the compressive stresses generated by the martensitic transformation (b) $K_{max\ trans}$ and $K_{min\ trans}$ *vs.* Fatigue crack growth rate.

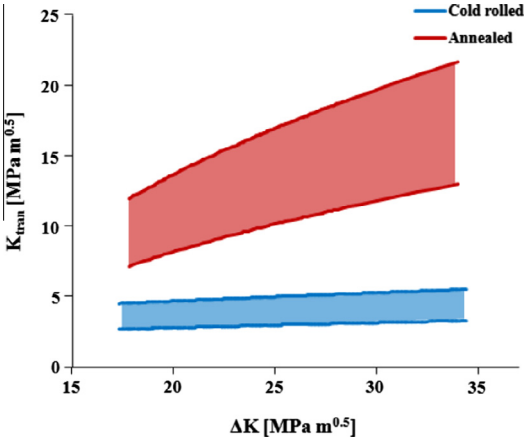

Fig. 17. Stress intensity factor caused by the martensitic transformation *vs.* range of stress intensity factor.

The inconvenience of the last proposed solution lies in the fact that when the value of α_n is calculated, it becomes bigger than 1 losing its physical meaning. Another observation obtained based on this solution is that the crack closure induced by the martensitic transformation in the annealed steel should be much higher than the obtained in the cold rolled steel, as can be seen in the values of (K_{min}–K_{tran}) in Fig. 16b. Considering that the residual stress measured by Rajanna et al. [32] are taken from the surface fracture of an MASS with subcritical martensitic transformation, and taking into account the results obtained in Fig. 16a, it is probable that the residual stresses induced by the martensitic transformation in the crack wake are partially responsible for the differences in the FCGR between the MASS in the annealed and cold rolled conditions used in this investigation.

Another factor that should be considered when explaining the differences in the FCGR between the MASS in annealed and cold rolled condition is the damage distribution around the crack tip. To understand the micromechanism of crack growth in this steel, SEM images of the fracture surface of the different condition tested are shown in Fig. 18.

6.3. Fracture surfaces analysis

In all cases, the observed fracture mode is transgranular without striations. The comparison between the SEM images obtained to a load ratio of 0.1 for the steel in annealed and cold rolled condition, Fig. 18a and c, shows that the principal difference in the crack advance mechanism between the two alloys is the large number of micro cracks present in the surface fracture of the cold

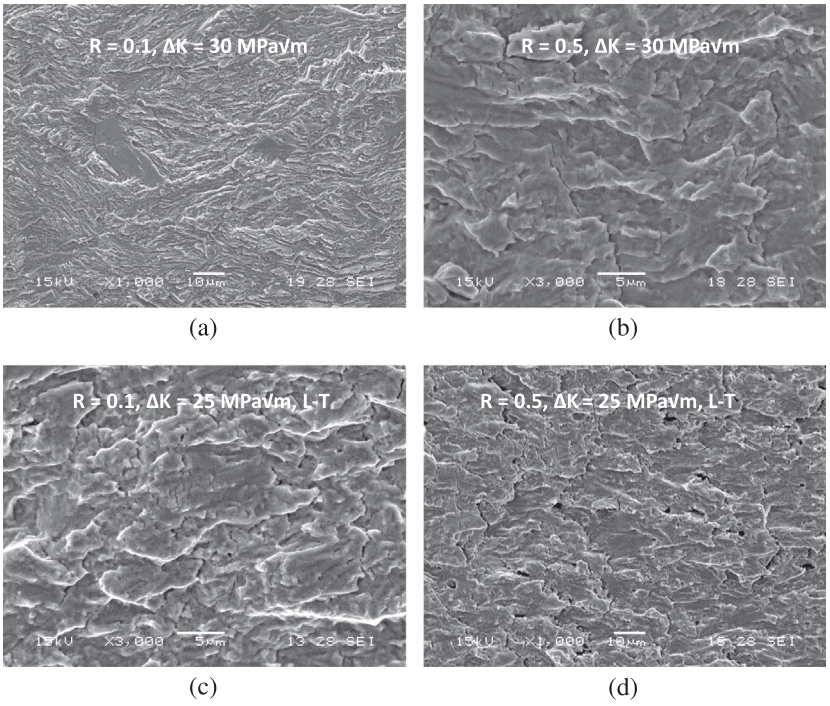

Fig. 18. SEM image of the fatigue fracture surface corresponding to (a and b) annealed steel, (c and d) cold rolled steel.

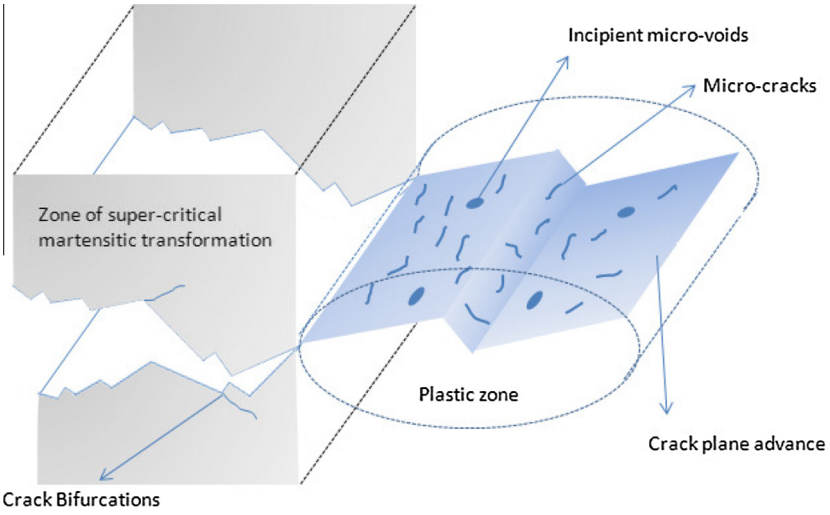

Fig. 19. Schematic illustration of the micro cracks and the incipient micro voids coalescing with the main crack.

rolled steel. According to previous studies, the fatigue crack nucleation in the regime of low cycle fatigue, where the plastic deformation is large as in the plastic zone, occurs exclusively within the martensite phase both in the surface and in the bulk of the specimen [33]. The effect of microcracks in the FCGR is varied; the linear elastic analyses of bifurcated cracks performed by Suresh [34] shows that for the same crack length, the effective stress intensity factor is lower for branched cracks than for straight cracks. However, microcracks can increase the FCGR if they coalesce with main crack, creating a reduction in the crack path [35]. Fig. 19 schematically shows the effect of the micro cracks in the crack path. These micro cracks are also present in the steel in annealed state tested to an R value equal to 0.5, although the nucleation of these micro cracks is related to the increase in $K_{max,}$ (see Fig. 18b). With the increase in K_{max} in the steel in the cold rolled condition, both mechanisms of micro crack nucleation previously explained are present together with the formation of incipient micro voids, (see Fig. 18d).

As the explanation of the FCGR decrease is based on the compressive stress field caused by the martensitic transformation, in which the effect of the residual stress is accounted in the applied driving force by modifying the contribution of K_{max} to the crack advance, the K_{max} parameter plays a fundamental role in the mechanism of fatigue crack advance of MASS and in the explanation of the lower FCGR of the annealed steel compared to the cold rolled steel. However, it is expected that if the lower FCGR in MASS compared to other alloys were caused only by the fracture mode, especially in the steel in annealed state, the surface fracture morphology should have a more ductile appearance. However, as general characteristic, fracture surfaces are quasi-brittle, which is

attributed to the complete martensitic transformation in the zone adjacent to the crack.

7. Conclusions

A new stress intensity factor solution (K) is proposed for the SENT specimens of this investigation. This solution could be used as a possible explanation to the uncommon applied stress effect observed, in previous studies, in thin sheet specimens of MASS.

The FCGR curves have also been evaluated in terms of the ΔK_{eff}. The results show that, according to the offset used to measure the point where the crack faces make contact, the correlation of the load ratio effects can be improved or worsened. However, the correlation of the load effects using Kujawski's parameter is superior. For the annealed specimens, the suitable value for α equals 0.6 and for the cold rolled specimens, 0.7.

The exceptional FCGR of MASS has an explanation in the mechanism of the residual stress induced by the martensitic transformation, and the appearance of a quasi-static fracture mode such as micro-crack formation and incipient micro-voids. In this context, it is worth noting that the increase of the crack propagation resistance of the annealed steel compared to cold rolled steel is not only caused by the austenite transformed to martensite prior the tests, but also, by the increase in the size of the zone transformed to martensite attendant to the test in the annealed specimens.

Finally, a parameter that takes into account the effect of residual stress is proposed. This new parameter is based on the two-driving force concept for fatigue crack advance (K_{max} and ΔK).

Acknowledgements

Authors wish to express their gratitude to the funding provided by CONICET (Consejo Nacional de Investigaciones Científicas y Técnicas), and by Agencia Nacional de Promoción Científica y Tecnológica, Argentina (PICT2010 Nro. 0379).

References

[1] Talonen J. Effect of strain-induced α′-martensite transformation on mechanical properties of metastable austenitic stainless steel. Doctoral dissertation; 2007.
[2] Pineau AG, Pelloux RM. Influence of strain-induced martensitic transformations on fatigue crack growth rates in stainless steels. Metall Trans 1974;5(5):1103–12. http://dx.doi.org/10.1007/BF02644322.
[3] Mei Z, Morris JW. Influence of deformation-induced martensite on fatigue crack propagation in 304-type steels. Metall Trans A 1990;21(12):3137–52. http://dx.doi.org/10.1007/BF02647310.
[4] Schuster G, Altstetter C. Fatigue of annealed and cold worked stable and unstable stainless steels. Metall Trans A 1983;14(10):2077–84. http://dx.doi.org/10.1007/BF02662374.
[5] Biswas Somjeet, Sivaprasad S, Narasaiah N, Tarafder S, Chakraborti PC. Load history effect on FCGR behaviour of 304LN stainless steel. Int J Fatigue 2007;29(4):786–91. http://dx.doi.org/10.1016/j.ijfatigue.2006.06.003.
[6] Chanani GR, Antolovich, Stephen D, Gerberich WW. Fatigue crack propagation in trip steels. Metall Trans 1972;3(10):2661–72. http://dx.doi.org/10.1007/BF02644242.
[7] Head AK. The growth of fatigue cracks. London, Edinburgh, Dublin Philos Mag J Sci 1953;44(356):925–38. http://dx.doi.org/10.1080/14786440908521062. XCVIII, Series 7.
[8] Rickerby DG, Fenici P. Fatigue crack growth in thin section type 316 stainless steel. Eng Fract Mech 1984;19(4):585–99. http://dx.doi.org/10.1016/0013-7944(84)90092-4.
[9] Nebel Th, Eifler D. Cyclic deformation behaviour of austenitic steels at ambient and elevated temperatures. Sadhana 2003;28(1–2):187–208.
[10] Hartmann HR, Churchill RW. KRAK-GAGE: a new transducer for crack growth measurement. Presented at the society for experimental stress analysis fall meeting, sponsored by the society for experimental stress analysis; 1981.
[11] ASTM E 647-08e1. Standard test method for measurement of fatigue crack growth rates. Annual book of ASTM standards; 2010.
[12] Park J, Song J, Earmme Y, Kim C. Personal computer based fatigue testing automation and improvement in fatigue behavior monitoring. Trans KSME 1988;12:123–30.
[13] Kim Chung-Youb, Song Ji-Ho. An automated procedure for determining crack opening level from differential displacement signal data. Int J Fatigue 1993;15(4):301–9. http://dx.doi.org/10.1016/0142-1123(93)90379-5.
[14] Chung Youn-Il, Song Ji-Ho. Improvement of ASTM compliance offset method for precise determination of crack opening load. Int J Fatigue 2009;31(5):809–19. http://dx.doi.org/10.1016/j.ijfatigue.2008.11.006.
[15] Paris PC, Gomez M, Anderson WE. A rational analytic theory of fatigue. Trend Eng Univ Washington 1961;13(1):9–14.
[16] Adair BS, Johnson WS, Antolovich SD, Staroselsky A. Temperature and load interaction effects on the fatigue crack growth rate and fracture surface morphology of IN100 superalloy. In: 38th National symposium on fatigue and fracture mechanics; 2011, May 18–May 20.
[17] John R, Kaldon SG, Johnson DA, Coker D. Weight function for a single edge cracked geometry with clamped ends. Int J Fract 1985;72(2):145–58. http://dx.doi.org/10.1007/BF00042825.
[18] Tada Hiroshi, Paris PC, Irwin GR. The analysis of cracks handbook. New York: ASME Press; 2000.
[19] Kujawski Daniel. A fatigue crack driving force parameter with load ratio effects. Int J Fatigue 2001;23:239–46. http://dx.doi.org/10.1016/S0142-1123(01)00158-X.
[20] Gray GT, Williams JC, Thompson AW. Roughness-induced crack closure: an explanation for microstructurally sensitive fatigue crack growth. Metall Trans A 1983;14(2):421–33. http://dx.doi.org/10.1007/BF02644220.
[21] Elber W. The significance of fatigue crack closure. ASTM STP 486. Damage tolerance in aircraft structures; 1971. p. 230–42.
[22] Suresh S. Crack deflection: implications for the growth of long and short fatigue cracks. Metall Trans A 1983;14(11):2375–85. http://dx.doi.org/10.1007/BF02663313.
[23] Noroozi AH, Glinka G, Lambert S. Prediction of fatigue crack growth under constant amplitude loading and a single overload based on elasto-plastic crack tip stresses and strains. Eng Fract Mech 2008;75(2):188–206. http://dx.doi.org/10.1016/j.engfracmech.2007.03.024.
[24] Beese AM, Mohr Dirk. Identification of the direction-dependency of the martensitic transformation in stainless steel using in situ magnetic permeability measurements. Exp Mech 2011;51(5):667–76. http://dx.doi.org/10.1007/s11340-010-9374-y.
[25] Talonen J, Aspegren P, Hänninen H. Comparison of different methods for measuring strain induced α-martensite content in austenitic steels. Mater Sci Technol 2004;20(12):1506–12. http://dx.doi.org/10.1179/026708304X4367.
[26] Schuster Gary, Altstetter Carl. Comparison of fatigue damage in stable and unstable stainless steels. ASTM STP 1983;811:445–63.
[27] Antolovich Stephen D, Singh Birindar. Observations of martensite formation and fracture in TRIP steels. Metall Mater Trans B 1970;1(12):3463–5. http://dx.doi.org/10.1007/BF03037885.
[28] Beese Allison M, Mohr Dirk. Effect of stress triaxiality and Lode angle on the kinetics of strain-induced austenite-to-martensite transformation. Acta Mater 2011;59(7):2589–600. http://dx.doi.org/10.1016/j.actamat.2010.12.040.
[29] Mcmeeking RM, Evans AG. Mechanics of transformation-toughening in brittle materials. J Am Ceram Soc 1982;65(5):242–6. http://dx.doi.org/10.1111/j.1151-2916.1982.tb10426.x.
[30] Reed RP. The spontaneous martensitic transformations in 18% Cr, 8% Ni steels. Acta Metall 1962;10(9):865–77. http://dx.doi.org/10.1016/0001-6160(62)90101-3.
[31] Paris P, Mcmeeking M, Tada H. The weight function method for determining stress intensity factors. Cracks Fract 1975:471–89. ASTM STP 601.
[32] Rajanna K, Pathiraj B, Kolster BH. X-ray fractography studies on austenitic stainless steels. Eng Fract Mech 1996;54(1):155–66. http://dx.doi.org/10.1016/0013-7944(95)00246-4.
[33] Stolarz Jacques, Baffie Natacha, Magnin Thierry. Fatigue short crack behavior in metastable austenitic stainless steels with different grain sizes. Mater Sci Eng, A 2001;319:521–6. http://dx.doi.org/10.1016/S0921-5093(01)01072-3.
[34] Suresh S. Micromechanisms of fatigue crack growth retardation following overloads. Eng Fract Mech 1983;18(3):577–93. http://dx.doi.org/10.1016/0013-7944(83)90051-6.
[35] Pokluda Jaroslav, Sandera Pavel. Micromechanisms of fracture and fatigue. s.l.: Springer; 2010. http://dx.doi.org/10.1007/978-1-84996-266-7.